A Prediction-Based Current Sampling Scheme Using Three Resistors for Induction Motor Drives

Ziyi Li and Qiang Gao

***Abstract*—In the traditional three-resistor-based current sampling scheme, the sampled currents will become inaccurate when the duration of zero-voltagevectors of an inverter is too short, which leads to a limited modulation index (MI). To overcome this problem, an improved three-resistor sampling method is proposed by establishing a predictive current model of an inverter load, which is that of an induction motor on the synchronous rotating frame for the demonstration purpose in this paper. The principle of this method is detailed in the paper. Then a simulation model of a vector-controlled induction motor drive that utilizes the proposed current sampling scheme is built in the Simulink environment. Finally, the experiment on the new sampling scheme is performed in both steady-state and dynamic conditions. The results verify that the existing current sampling problems can be solved effectively and the motor can perform well with higher MI under the new scheme. As a result, the loading capacity of the system can be enhanced notably.**

***Index Terms*—And vector control, Induction motor, inverter, predictive current model, three-resistor current sampling scheme.**

I. Introduction

FOR a closed-loop current control of an inverter, no matter what control scheme is applied, e.g., a PI controller [1], [2] or a hysteresis controller [3], [4], etc., it is important that the feedback currents are accurately measured. Mostly, the load currents of an inverter are measured by current sensors, for example, hall-effect sensors and current transducers [5]–[7]. But due to the relatively large package and high price of these current sensors, they are normally not suitable for small PCBs and low-cost applications. Consequently, a type of current sampling schemes using resistor(s) or fewer current sensors [8]–[16] for inverters have been proposed to reduce the volume and the cost.

These resistor sampling systems can be generally divided into two categories:

1) Single-resistor sensing system is shown in Fig. 1 [8]. The load currents are reconstructed by the sampled dc currents the are obtained through the sampling resistor between the rectifier and the dc link. The dc currents are sampled twice during two consecutive active voltage vectors for a three-phase two-level voltage-source inverter (VSI) in a pulsewidth modulation (PWM) period. It uses the information in the two active voltage vectors to obtain two output currents and the third can easily be calculated [9], [10]. When the dwell time of each measuring active vector is shorter than the minimum sampling time $T_{\min}$ (about 3–5 μs), which is determined by the A/D sampling and conversion time and dead time of PWMs, the sampled currents will be inaccurate, thus leading to poor control performance or even instability [11]. In order to address the problem, some researchers proposed some improved solutions to reconstruct three phase currents, such as the measurement vector insertion method and modified PWM strategy [12]–[14]. These methods are effective, but they need complex mathematical calculation and logical judgment, and will induce more harmonics.
2) Three-resistor sampling system is shown in Fig. 2 [15]. The load currents are gained by the three sampling resistors that are installed between the low-side power switches of the inverter and the ground. Fig. 2 shows the schematic

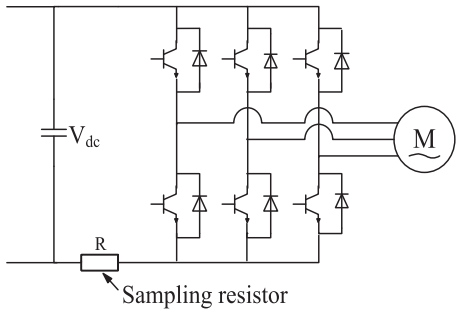

Fig. 1. Single-resistor current sampling system.

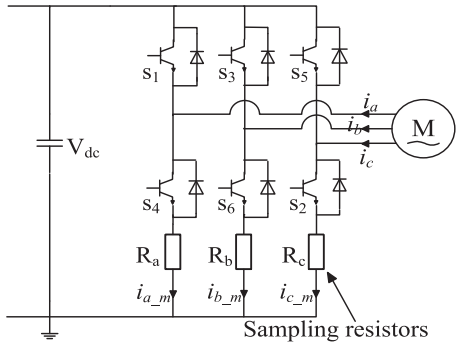

Fig. 2. Three-resistor current sampling system.

Manuscript received March 6, 2016; revised May 24, 2017; accepted August 4, 2017. Date of publication August 14, 2017; date of current version March 5, 2018. Recommended for publication by Associate Editor Prof. Ralph Kennel. *(Corresponding author: Qiang Gao.)*

The authors are with the Department of Electrical Engineering, Shanghai Jiao Tong University, Shanghai 200240, China (e-mail: 565039062@qq.com; gaoqiang@sjtu.edu.cn).

Color versions of one or more of the figures in this paper are available online at http://ieeexplore.ieee.org.

Digital Object Identifier 10.1109/TPEL.2017.2740361

of the scheme in the case of a three-phase two-level VSI feeding a motor. The sampling process needs to be finished during the duration of a zero-voltage vector, T_0, in a PWM cycle. Compared with the single-resistor sensing method, it is much simpler to reconstruct the load current and also easier to realize the protection of the power electronic modules. But just like the previous method, the problem of inaccurate sampled currents also exists due to the minimum sampling time $T_{\min}$. Paper [16] proposed a state observer and a fuzzy-logic-function-based scheme to reconstruct phase currents of PMSM when T_0 is too short, but the above problems in the case of an ACIM load still exist.

In this paper, aiming at solving the problems in the three-resistor sampling scheme, an improved current reconstruction and control method based on the predictive current model of the inverter's load is presented. In addition, a model of the scheme, when applied to an induction motor drive, is established in the MATLAB/Simulink. Finally, the experiments based on the TMS320F28069M are performed in both steady-state and dynamic conditions, and the wider range closed-loop control of an induction motor is realized under the improved current sampling approach.

II. Traditional Three-Resistor Current Sampling Scheme

A. Principle of the Traditional Three-Resistor Current Sampling Scheme

The topology of the three-resistor current sampling system is shown in Fig. 2. R_a, R_b, and R_c are the three sampling resistors that should meet certain requirements: small enough resistance, high precision, good stability, and so on [17]. The real motor currents are represented by i_a, i_b, and i_c, while i_{a_m}, i_{b_m}, and i_{c_m} are the three sampled currents through the resistors. For simplicity, their positive directions are defined as indicated by the arrows in the figure.

In this system, the currents are sensed during the zero vector (000). For phase A, i_a passes through the low-side switch S_4 and the resistor R_a when S_4 turns on within the zero vector. In this case, we can obtain $i_a = i_{a\_m}$. After the zero vector, i_a will not be equal to i_{a_m} because S_4 turns off so that i_a flows through the freewheel diode in the high-side switch. Similarly, the currents i_b and i_c can be obtained when S_6 and S_2 are on. Therefore, only in the zero-voltage vector can all three-phase currents of the motor be constructed as

$$i_a = i_{a\_m},\ i_b = i_{b\_m},\ i_c = i_{c\_m}\,. \tag{1}$$

The sampling process are described by taking Sector I as an example in Fig. 3. Let T_1, T_2, T_3 represent three-phase PWM comparison values, and we define the duration of the zero vector as T_0 and $T_0 = \min\{T_1, T_2, T_3\}$. At the beginning of the zero vector during every PWM period, the A/D sampling is triggered and three currents i_{a_m}, i_{b_m}, and i_{c_m} are sampled and stored in the DSP. From (1), i_a, i_b, and i_c can be obtained and used for the closed-loop control.

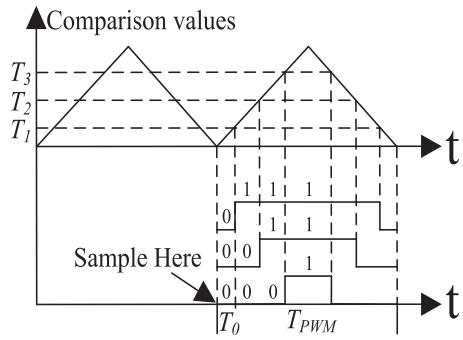

Fig. 3. Three-resistor sampling process in Sector I.

B. Problems of Traditional Three-Resistor Current Sampling Scheme

In the above analysis of Section A, the deficiency of the zero vector's dwell time, T_0, is not considered. Taking into account the A/D sampling and conversion time $(t_{\rm conv})$, dead time (t_d) and the stabilizing time $(t_{\rm stab})$ of the resistor current, the minimum $T_{0,,}$i.e., $T_{\min}$, is expressed as [11]

$$T_{\min} = t_{\rm conv} + t_d + t_{\rm stab}. \tag{2}$$

In this paper, the modulation index (MI) is defined as the ratio of the amplitude of the reference voltage vector $U_{\rm ref}$ to the radius of the inscribed circle of the vector hexagon $U_{\rm base}$, given by

$$\mathrm{MI} = U_{\rm ref}/U_{\rm base}. \tag{3}$$

Replacing $U_{\rm ref}$ and $U_{\rm base}$ with the duration of the voltage vector in Fig. 3, (3) is rewritten as

$$\mathrm{MI} = 1 - T_0 \times 4/T_{\rm PWM}. \tag{4}$$

When the duration of the zero vector T_0 is shorter than $T_{\min}$, the sampling process cannot be completed and the sampled currents will be inaccurate. In other words, the MI cannot reach 1 under the traditional three-resistor current sampling scheme. For instance, if the frequency of the PWM is 15 kHz and $T_{\min}$ is 3 μs in a control system, its MI should not be more than 0.82. In view of the minimum sampling time, there are three conditions of obtaining motor currents under three-resistor sampling method. Taking Sector I as an example, the three conditions can be described as follows [18]:

MODE 1: $T_1 > T_{\min}$. During the zero vector, all the three resistor currents are sampled completely and accurately. Three-phase currents of the motor can be obtained directly by (1).

MODE 2: $T_1 < T_{\min}$, $T_{2,3} > T_{\min}$. The resistor currents of phase B and phase C are accurate within the zero vector. Three-phase currents of the motor can be obtained indirectly.

MODE 3: $T_{1,2} < T_{\min}$, $T_3 > T_{\min}$. Only the resistor current of phase C is accurate. Three-phase currents of the motor cannot be reconstructed.

Under the traditional three-resistor current sampling scheme, the three-phase currents of the motor cannot be obtained directly in MODE 2 and MODE 3. Aiming at MODE 2, i_b and i_c are

TABLE I
CURRENT RELATIONSHIPS IN ALL THE THREE MODES

Current Relationships		i_a	i_b	i_c
$T_1 > T_{\min}$	$T_{2,3} > T_{\min}$	i_{a_m}	i_{b_m}	i_{c_m}
$T_1 < T_{\min}$	$T_{2,3} > T_{\min}$	$-i_{b\_m} - i_{c\_m}$	i_{b_m}	i_{c_m}
$T_2 < T_{\min}$	$T_{1,3} > T_{\min}$	i_{a_m}	$-i_{a\_m} - i_{c\_m}$	i_{c_m}
$T_3 < T_{\min}$	$T_{1,2} > T_{\min}$	i_{a_m}	i_{b_m}	$-i_{a\_m} - i_{b\_m}$
$T_{1,2} < T_{\min}$	$T_3 > T_{\min}$	—	—	i_{c_m}
$T_{1,3} < T_{\min}$	$T_2 > T_{\min}$	—	i_{b_m}	—
$T_{2,3} < T_{\min}$	$T_1 > T_{\min}$	i_{a_m}	—	—

valid and i_a can be calculated as

$$i_a = -i_b - i_c = -\left(i_{b\_m} + i_{c\_m}\right). \tag{5}$$

Extending to all the sectors of SVPWM, the current relations between the real motor currents and the sampled resistor currents are listed in Table I. In the table, "—" means that the value cannot be obtained.

From above analysis, when MI is high and zero vector T_0 is not long enough to finish the complete sampling, the three-phase currents of the motor will be distorted, so the current closed-loop's control performance will degrade. In severe cases, the motor will vibrate violently and generate high noise leading to undesired structural damage.

III. IMPROVED THREE-RESISTOR CURRENT SAMPLING SCHEME

A. The Predictive Current Model of an IM

The proposed current sampling scheme is based on the predictive current model of an induction motor in the synchronous rotating frame. In the orthogonal $\underline{d}$–$\underline{q}$ axis, the $\psi_r - i_s$ model of an IM can be given by [19]

$$\begin{aligned}
\frac{di_{sd}}{dt} &= \frac{L_m}{\sigma L_s L_r T_r}\psi_{rd} + \frac{L_m}{\sigma L_s L_r}\omega\psi_{rq} - \frac{R_s L_r^2 + R_r L_m^2}{\sigma L_s L_r^2} i_{sd} \\
&\quad + \omega_1 i_{sq} + \frac{u_{sd}}{\sigma L_s} \\
\frac{di_{sq}}{dt} &= \frac{L_m}{\sigma L_s L_r T_r}\psi_{rq} - \frac{L_m}{\sigma L_s L_r}\omega\psi_{rd} - \frac{R_s L_r^2 + R_r L_m^2}{\sigma L_s L_r^2} i_{sq} \\
&\quad - \omega_1 i_{sd} + \frac{u_{sq}}{\sigma L_s} \\
\frac{d\psi_{rd}}{dt} &= -\frac{1}{T_r}\psi_{rd} + (\omega_1 - \omega)\psi_{rq} + \frac{L_m}{T_r} i_{sd} \\
\frac{d\psi_{rq}}{dt} &= -\frac{1}{T_r}\psi_{rq} - (\omega_1 - \omega)\psi_{rd} + \frac{L_m}{T_r} i_{sq}
\end{aligned} \tag{6}$$

where $\sigma = 1 - L_m^2/L_s L_r, T_r = L_r/R_r$. The meaning of each variable in (6) is explained in Table II.

In the practical control system, the model are treated with its discrete form. Generally, the sampling frequency is much larger than the fundamental frequency. Therefore, the state equations can be discretized as follows:

$$\begin{aligned}
\frac{i_{sd}(k+1) - i_{sd}(k)}{T_s} &= \frac{L_m \psi_{rd}(k)}{\sigma L_s L_r T_r} + \frac{L_m \omega(k)\psi_{rq}(k)}{\sigma L_s L_r} \\
&\quad - \frac{\left(R_s L_r^2 + R_r L_m^2\right) i_{sd}(k)}{\sigma L_s L_r^2} \\
&\quad + \omega_1 i_{sq}(k) + \frac{u_{sd}(k)}{\sigma L_s} \\
\frac{i_{sq}(k+1) - i_{sq}(k)}{T_s} &= \frac{L_m \psi_{rq}(k)}{\sigma L_s L_r T_r} - \frac{L_m \omega(k)\psi_{rd}(k)}{\sigma L_s L_r} \\
&\quad - \frac{\left(R_s L_r^2 + R_r L_m^2\right) i_{sq}(k)}{\sigma L_s L_r^2} \\
&\quad - \omega_1(k) i_{sd}(k) + \frac{u_{sq}(k)}{\sigma L_s} \\
\frac{\psi_{rd}(k+1) - \psi_{rd}(k)}{T_s} &= -\frac{\psi_{rd}(k)}{T_r} + [\omega_1(k) - \omega(k)]\psi_{rq}(k) \\
&\quad + \frac{L_m}{T_r} i_{sd}(k) \\
\frac{\psi_{rq}(k+1) - \psi_{rq}(k)}{T_s} &= -\frac{\psi_{rq}(k)}{T_r} - [\omega_1(k) - \omega(k)]\psi_{rd}(k) \\
&\quad + \frac{L_m}{T_r} i_{sq}(k).
\end{aligned} \tag{7}$$

In the rotor-flux-oriented vector control, there is $\psi_{rq} = 0$ and $\psi_{rd} = L_m i_{sd}$. Applying them into (7) and performing the transformation, the predictive current model of the IM can be obtained as

$$\begin{aligned}
i_{sd}(k+1) &= \left(1 - \frac{R_s T_s}{\sigma L_s}\right) i_{sd}(k) + \omega_1(k) T_s i_{sq}(k) \\
&\quad + \frac{T_s}{\sigma L_s} u_{sd}(k) \\
i_{sq}(k+1) &= -\omega_1(k) T_s i_{sd}(k) - \frac{L_m^2 \omega(k) T_s}{\sigma L_s L_r} i_{sd}(k) \\
&\quad + \frac{T_s}{\sigma L_s} u_{sq}(k) \\
&\quad + \left(1 - \frac{R_s L_r^2 + R_r L_m^2}{\sigma L_s L_r^2} T_s\right) i_{sq}(k).
\end{aligned} \tag{8}$$

From (8), it can be seen that using the information of $i_{sd}(k)$, $i_{sq}(k), u_{sd}(k), u_{sq}(k), \omega_1(k)$ and $\omega(k), i_{sd}(k+1)$, and $i_{sq}(k+1)$ in the next PWM cycle can be predicted.

B. Improved Three-Current Sampling Scheme

According to (8), when only one sampled current is accurate and valid, we can calculate the desired currents for the closed-loop current control from the present information. Fig. 4 shows the block diagram of the rotor flux oriented control of the IM based on the improved three-resistor current sampling scheme. In the figure, the observer that gets information of voltages and currents from the motor is used to estimate the speed feedback

TABLE II
VARIABLES DEFINITION

Variables	Definition	Variables	Definition
R_s	Stator resistance	u_{sd}	stator voltage in d-axis
R_r	Rotor resistance	u_{sq}	stator voltage in q-axis
L_m	Magnetizing inductance	ψ_{rd}	flux linkage in d-axis
L_s	Stator inductance	ψ_{rq}	flux linkage in q-axis
L_r	Rotor inductance	ω_1	angular velocity of the reference frame
i_{sd}	Stator current in d-axis	ω	angular velocity of the rotor
i_{sq}	Stator current in q-axis		

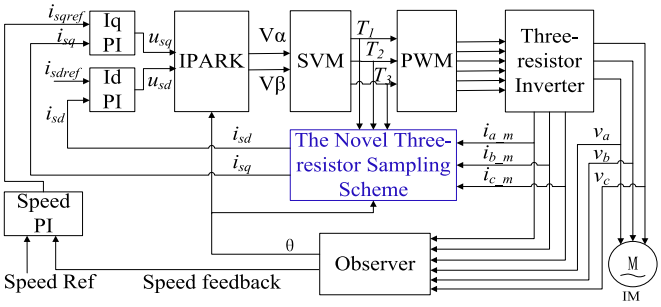

Fig. 4. Rotor-flux-oriented control based on the improved three-resistor sampling scheme.

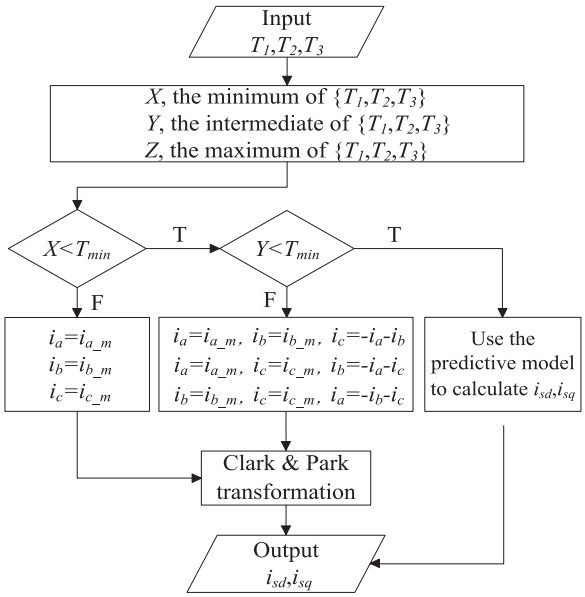

Fig. 5. Flowchart of the improved three-resistor sampling scheme based on the predictive current model.

and rotor position [20]. The details of the new sampling scheme are given in Fig. 5.

In every PWM cycle, we use X, Y, Z to replace T_1, T_2, T_3, and $X \le Y \le Z$. Depending on the different relation between X, Y, Z, and $T_{\min}$, i_{sd} and i_{sq} can be obtained in different ways:

1) $X \ge T_{\min}$. During the zero vector, all the three resistor currents are sampled completely and accurately. Three-phase currents of the motor can be obtained directly. I_{sd} and i_{sq} can be obtained through Clark and Park transformation.
2) $X \le T_{\min}$, $Y \ge T_{\min}$. There are two accurate resistor currents within the zero vector. Three-phase currents of the motor can be obtained indirectly via (5). I_{sd} and i_{sq} can be obtained through Clark and Park transformation.
3) $X \le T_{\min}$, $Y \le T_{\min}$, $Z \ge T_{\min}$. Only one resistor current is accurate. Using the predictive current model, i_{sd} and i_{sq} can be calculated from the present values of the variables. Particularly, the three-phase currents of the motor i_a, i_b, and i_c can be reconstructed by inverse Park and inverse Clark transformation.

This improved three-resistor sampling scheme can be used in many motor control applications, including the sensorless operation. Generally, the currents can be sampled accurately by the resistors under the appropriate MI. At high MI where the zero vector's dwell time is not enough, the proposed sampling scheme based current prediction model will be used to reconstruct the phase currents.

IV. VALIDATION BY SIMULATION

With the aforementioned scheme, a simulation model of vector control of an induction motor has been established on the SIMULINK platform. The ACIM module is built through the state equations of induction motor, and the sampling module simulates the real sampling process of DSP which contains sample and hold of an A/D. The controller is established with the aid of the improved scheme.

In the simulation, the dc voltage is 310 V and the switching frequency of the IGBTs is 15 kHz. Considering the dead time, the sampling and conversion time, and so on, $T_{\min}$ is set to 3 μs in the simulation. Table III shows the parameters of the ACIM. For illustration, two ways of feedback for the current-loop control are implemented. One way is to use the real motor currents, which are gained from the measurement module of the Simulink; the other way is to use the sampled currents obtained from the proposed sampling scheme. Because the real currents come from the motor directly, they are assumed to have no errors, and the control with the feedback of real currents can be seen as the benchmark for comparison.

When the motor is running in the rated condition, the reference voltage vector reaches the inscribed circle of the hexagon so that the situation as described in MODE 3 in part II will appear. The FOC of the motor based on the improved three-

TABLE III
PARAMETERS OF THE ACIM

Parameter	Value
R_s	1.2 Ω
R_r	1.22 Ω
L_m	71.33 e − 3 H
L_s	78.86 e − 3 H
L_r	78.86 e − 3 H
n_p	2
Rated power	1.5 kW
Rated speed	1500 r/min

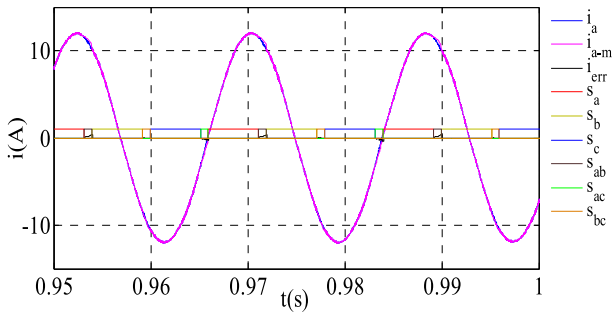

Fig. 6. Sampled current and motor current of phase A when the feedback currents are motor currents.

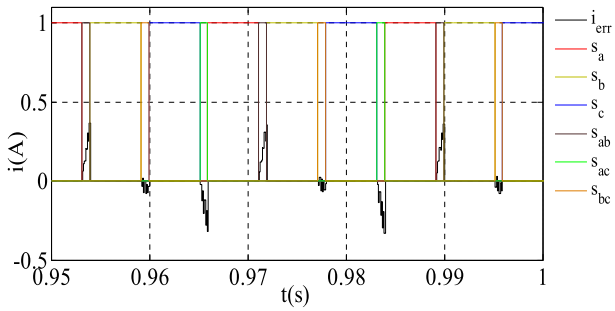

Fig. 7. Errors between the two currents when the feedback currents are motor currents.

resistor current sampling technology is simulated and analyzed from the following main aspects.

1) First, the real motor currents serve as the feedback currents to do the closed-loop control. In this case, the sampled currents exported by the improved sampling scheme are compared with the motor currents. Figs. 6 and 7 show the current waveform of phase A obtained by both methods and their errors. In the figures, i_a means the real motor current of phase A from the measurement module, and i_{a_m} is the sampled current of phase A from the improved sampling scheme, and $i_{\rm err}$ is the errors between the two currents. $s_a = 1$ means that two measured currents from the low-side resistors of phase B and phase C are valid, while $s_b = 1$ indicates that two resistor currents of phase A and C are valid and $s_c = 1$ means phase A and phase B. $s_{bc} = 1$, $s_{ac} = 1$, and $s_{ab} = 1$ mean that only one measured resistor current of phase A, phase B, and phase C is valid, respectively. From Fig. 7, the maximum absolute error (MAE) between the sampled current and the real motor current in all conditions are calculated as shown in Table IV. The biggest error is 0.294 A (3.47% based on rated current 8.47 A), which shows that the sampled current based on the improved sampling scheme is very close to the real motor current.
2) In this step, the feedback currents for the current-loop control are the sampled currents. Just like the first simulation, the waveform and the errors of the two currents are drawn in Figs. 8 and 9. Table IV shows the values of the maximum errors, and the maximum value of MAEs is only −0.393 A (4.64%), which occurs when $s_{ac} = 1$. From the table, the biggest error of Fig. 9 is slightly higher than that in Fig. 7.
3) The output currents of phase A from both ways are analyzed by FFT, as shown in Figs. 10 and 11. The results shows the comparable harmonic performance with the two different current feedbacks.

TABLE IV
ERRORS IN CERTAIN CONDITIONS

MAE	$s_a = 1$	$s_b = 1$	$s_c = 1$	$s_{ab} = 1$	$s_{ac} = 1$	$s_{bc} = 1$
$i_{\rm err}$ in Fig. 7	0	0	0	0.294 A	−0.292 A	−0.089 A
$i_{\rm err}$ in Fig. 9	0	0	0	0.390 A	−0.393 A	−0.104 A

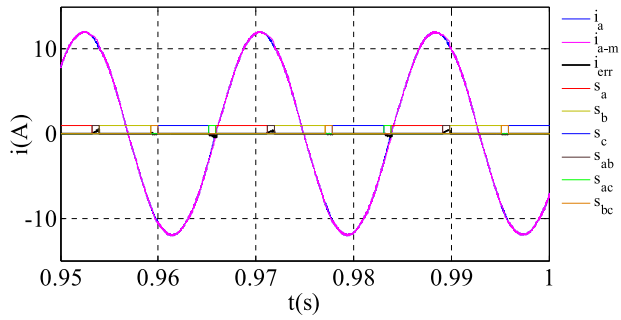

Fig. 8. Sampled current and motor current of phase A when the feedback currents are sampled currents.

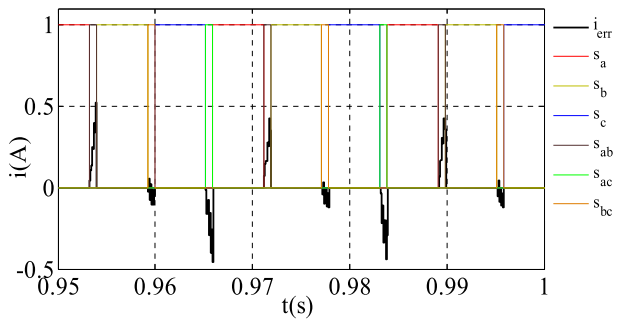

Fig. 9. Errors between the two currents when the feedback currents are sampled currents.

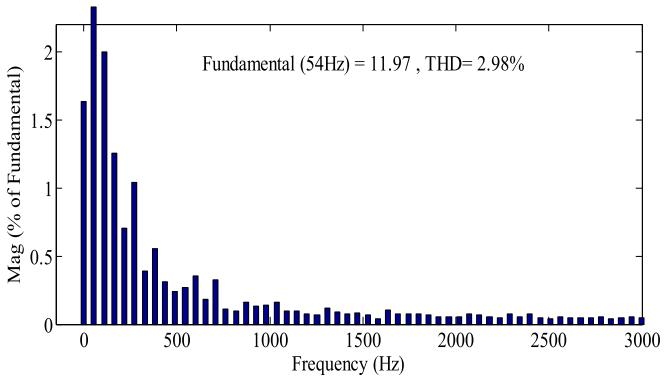

Fig. 10. FFT analysis of the output current of phase A when the feedback currents are motor currents.

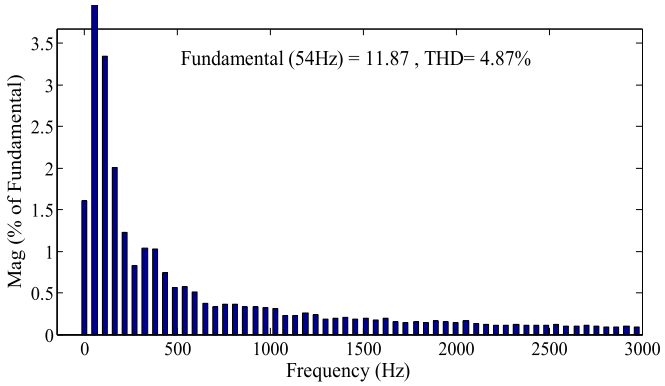

Fig. 11. FFT analysis of the output current of phase A when the feedback currents are sampled currents.

4) In the improved three-resistor sampling system, only one sampled current is accurate when the zero vector duration is too short. In this condition, the d–q currents used in the closed-loop control of the next interrupt cycle are calculated by the prediction model. So all the sampled currents in this situation would be useless to do the current-loop control. But from the prediction model, the results is dependent on the parameters of the motor. In order to investigate the effects of the motor parameters on the prediction model, the corresponding simulation experiment is built in both steady-state and dynamic conditions.

a) In the simulation, the stator resistance R_s of the prediction model is set to 1.8 time of the real value and the motor is set to the rated operation (1500 r/min, 9.55 N·m) with the sampled currents as the feedback currents. The waveform of sampled current and real motor current is shown in Fig. 12. Besides, their errors are shown in Fig. 13. Compared with the step 2 of simulation, the errors become larger because the predicted currents are inaccurate due to the changed stator resistance. In the figure, the max error is 1.07 A. By doing the FFT analysis of the output current of phase A when the feedback currents are sampled currents in the wrong value of R_s, the Total Harmonic Distortion (THD) is 6.23% and acceptable compared to 4.87% of Fig. 11. The results verify that the motor can perform well in the steady state even if the value of R_s in the prediction model is 1.8 times as much as the real value.

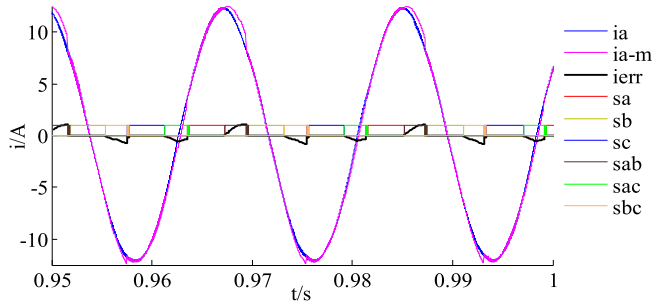

Fig. 12. Sampled current and motor current of phase A when the feedback currents are sampled currents ($R_s = 1.8^*$real R_s).

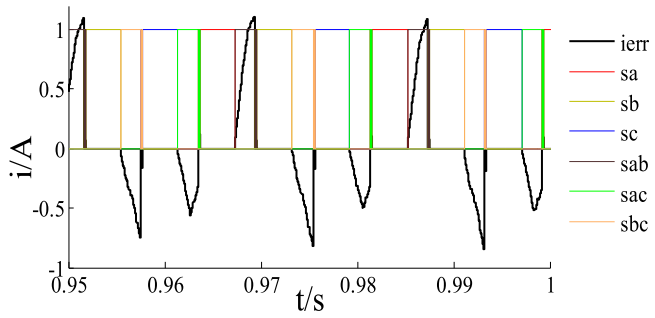

Fig. 13. Errors between the two currents when the feedback currents are sampled currents ($R_s = 1.8^*$real R_s).

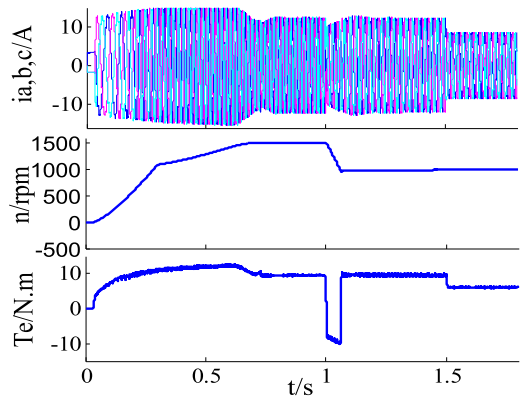

Fig. 14. Dynamic response of the ACIM based on the improved three-resistor sampling scheme ($R_s = 1.8^*$real R_s).

b) The dynamic experiment is simulated to verify and evaluate the dynamic response performance of improved sampling system under the changed parameters condition. Based on the aforementioned steady state of the motor, the speed and the torque dynamic simulation is built as shown in Fig. 14. At $t = 1$ s, the speed reference is changed from 1500 to 1000 r/min. The results verify that the motor can track the given speed and keep steady. Then the torque load is set to 6 N·m at $t = 1.5$ s, the system responds quickly and maintains the motor running at the constant speed. The simulation proves that the improved sampling system can perform well in the dynamic test.

TABLE V
RANGES OF PARAMETERS THAT CAN MAINTAIN THE ACIM STABLE

Parameter	Value
Stator resistance	$0.2\,R_s \sim 1.8R_s$
Rotor resistance	$0.65\,R_r \sim 1.13R_r$
Magnetizing inductance	$0.7\,L_m \sim 1.3\,L_m$
Stator inductance	$0.6\,L_s \sim 1.23\,L_s$
Rotor inductance	$0.6\,L_r \sim 1.23\,L_r$

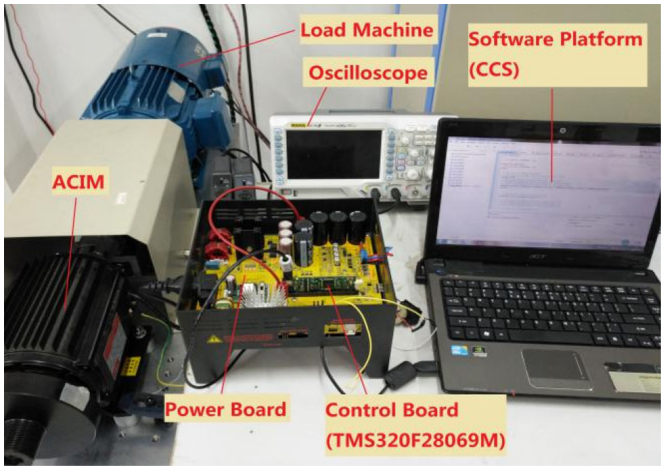

Fig. 15. Experimental platform of ACIM.

c) Besides the setting of stator resistance R_s, other parameters of the prediction model are also changed and set. Table V shows the acceptable ranges of these parameter values that can keep the motor operating and working well. In the practical application, the parameters of ACIM always change within these ranges. So the presented current prediction model with the changing parameters can be used into the motor control and has a good performance.

From the above simulation, it can be verified that the improved three-resistor sampling method performs well both in steady and in dynamic conditions, even with uncertain parameters.

V. VERIFICATION BY EXPERIMENT

The studied three-resistor current sampling algorithm has been implemented in an experimental ACIM drive. The experimental platform is shown in Fig. 15. The dc voltage from the uncontrolled single-phase rectifier has an amplitude of 310 V. The controller of TMS320F28069M is used for the algorithm implementation. The IPM of PS21765 (600 V, 20 A) is used for the inverter and the switching frequency is 15 kHz. Three sampling resistors are of 20 mΩ (1% of precision). Considering the dead time, the sampling and conversion time, and so on, $T_{\min}$ is set to 3 μs in the experiments. In the traditional three-resistor sampling system, the MI must be less than 0.82 to ensure that the sampled currents are accurate. Table VI shows the parameters of the ACIM, which is in delta connection.

TABLE VI
PARAMETERS OF THE ACIM

Parameter	Value
R_s	3.6 Ω
R_r	3 Ω
L_m	0.2139 H
L_s	0.2356 H
L_r	0.2356 H
n_p	2
Rated power	1.5 kW
Rated speed	1420 r/min

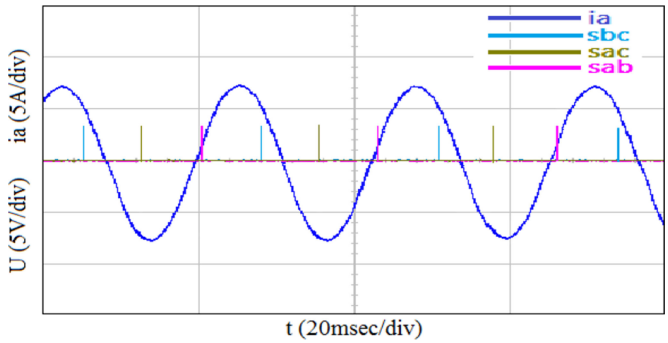

Fig. 16. Output motor current of phase A when the speed reference is1300 r/min without load under the improved sampling scheme.

TABLE VII
ERRORS IN CERTAIN CONDITIONS

Current Value	$s_{bc}=1$	$s_{ac}=1$	$s_{ab}=1$
Real value	5.210 A	−7.010 A	2.150 A
Predictive value	5.085 A	−6.833 A	2.066 A
Error	0.125 A	−0.177 A	0.084 A

The experiments contain steady-state and transient tests. All the feedback currents of current closed-loop control system are sampled currents through sampling resistors. The results are presented and analyzed from various aspects.

1) Fig. 16 shows the current waveform of phase A of the motor when it is running at 1300 r/min. Due to the limitation of the DSP, the predictive values of current are recorded only at the high-level of s_{bc}, s_{ac}, or s_{ab}. At the same time, the real values of current can be traced and read from the oscilloscope to be compared with the predictive values. The MAEs between the predictive values and the real values during the high-level period are given in Table VII. The maximum of MAEs is only −0.177 A (3.44% based on the RMS of 5.15 A), which occurs when $s_{ac}=1$. From the results, the phase current waveform can remain sinusoidal and the motor can be operated stably when the deficiency of duration of the zero vector occurs many times in one fundamental cycle.
2) To make a clear comparison between the traditional sampling scheme and the presented sampling scheme, the

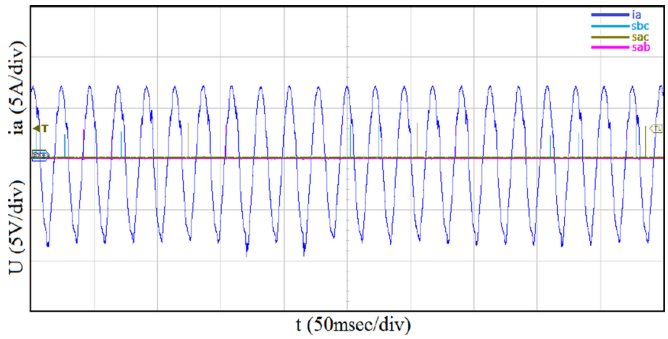

Fig. 17. Output motor current of phase A when the speed reference is1300 r/min without load under the traditional sampling scheme.

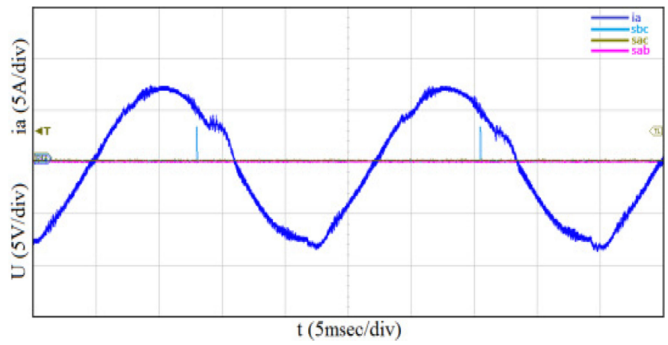

Fig. 18. Amplified waveform of i_a.

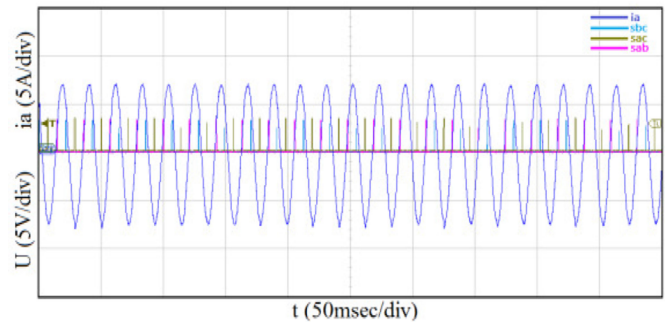

Fig. 19. Output motor current of phase A when the speed reference is 1400 r/min without load under the improved sampling scheme.

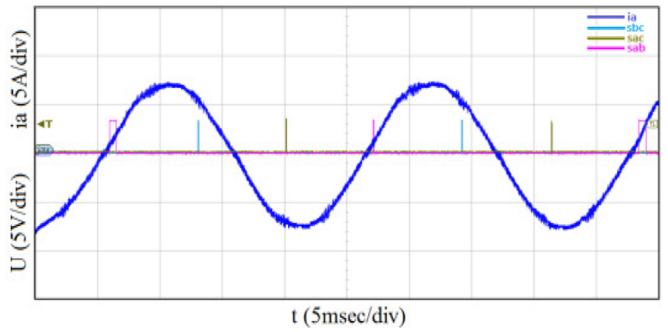

Fig. 20. Zoomed waveform of i_a.

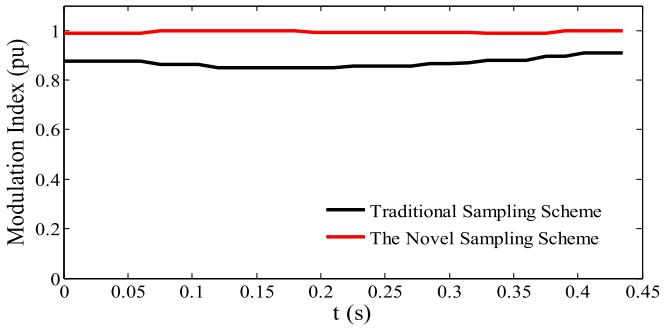

Fig. 21. MI in the two operation mode.

experiments of the two methods are done and the results are shown in Figs. 17–21.

In Fig. 17, the motor is running at 1300 r/min by the traditional sampling scheme. From the figure, the high-level states of s_{bc}, s_{ac}, or s_{ab} happen many times and last for some time in the given condition. Fig. 18 is the zoomed waveform of Fig. 17. The current waveform i_a appears obviously distorted as a result of the inaccuracy of the sampled currents. This means that the traditional three-resistor sampling scheme will not keep the motor running well when the duration of the zero vector is too short in high MI mode. In the experiment, the motor produces a very violent vibration and large noise.

In Fig. 19, the motor is running at 1400 r/min by the improved sampling scheme. From the figure, the high-level states of s_{bc}, s_{ac}, or s_{ab} happen more frequently in the given condition than the previous experiment at 1300 r/min. It indicates that the duration of zero vector is shorter and MI is higher. Fig. 20 is the zoomed waveform of Fig. 19. The current waveform i_a is sinusoidal and the system is more stable. From the experimental observation, the motor can work smoothly and no noise is produced.

Fig. 21 shows the waveform of MI in the two operation modes mentioned earlier. From the earlier analysis, the motor has not been able to keep the currents sinusoidal when the MI reaches about 0.86, as shown in the figure. Actually, the system under the traditional scheme could not work stably since the MI exceed 0.82. But using the improved sampling method, the MI can reach about 1 as the red line shows and the motor also works well.

3) Figs. 22 and 23 show the FFT analysis of the phase A's current of the motor. In order to make the comparison in the same condition, the two figures are all obtained at the speed of 1300 r/min without load. Fig. 22 is the FFT analysis under the traditional sampling scheme. The THD of the current is 10.96% which means the current contains rich harmonics because of the inaccurate sampling. Fig. 23 shows that the THD of current is only 3.48% when the motor is running under the improved scheme. Through the results, the harmonics can be greatly reduced without load by using the presented method.
4) In addition, the experiment results under load in comparison with the conventional sampling scheme are given in the following figures. Fig. 24 shows the output motor current of phase A with the traditional sampling scheme at

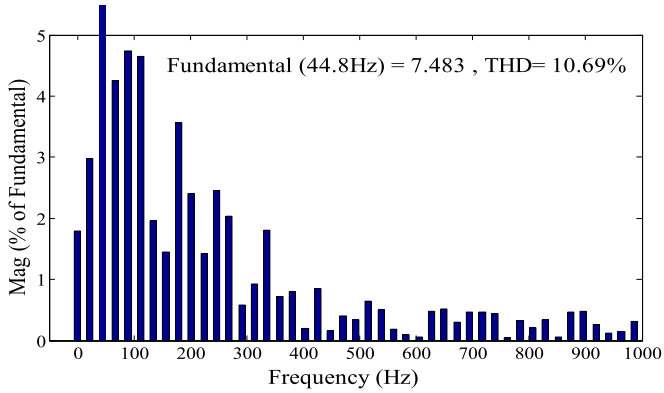

Fig. 22. FFT analysis of the output current of phase A under the traditional sampling scheme.

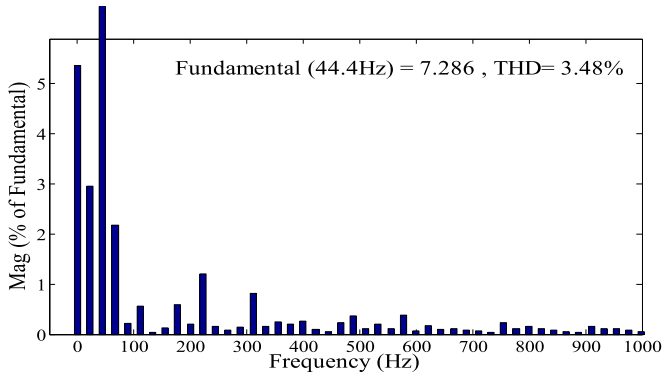

Fig. 23. FFT analysis of the output current of phase A under the improved sampling scheme.

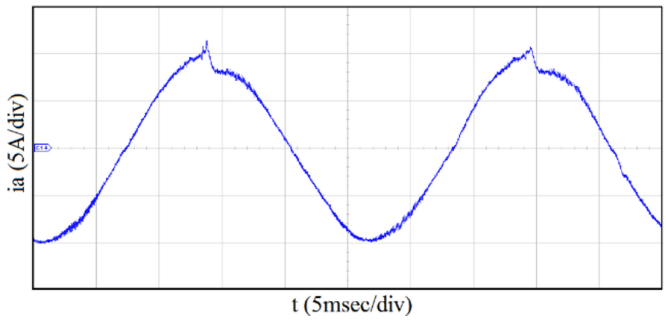

Fig. 24. Output motor current of phase A under the traditional sampling scheme ($n = 1100$ r/min, $T_e = 9$ N · m).

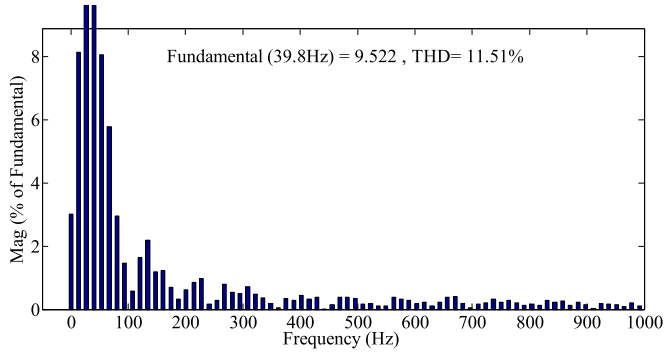

Fig. 25. FFT analysis of the output current of phase A under the traditional sampling scheme ($n = 1100$ r/min, $T_e = 9$ N · m).

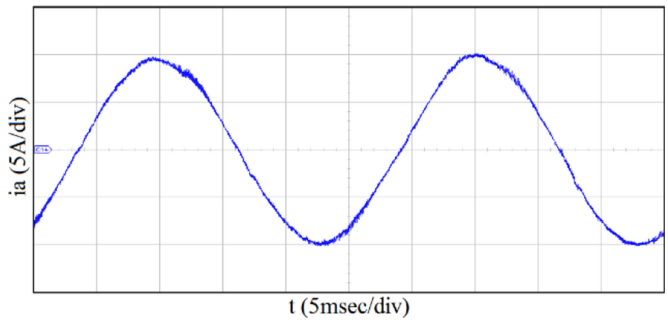

Fig. 26. Output motor current of phase A under the improved sampling scheme ($n = 1100$ r/min, $T_e = 9$ N · m).

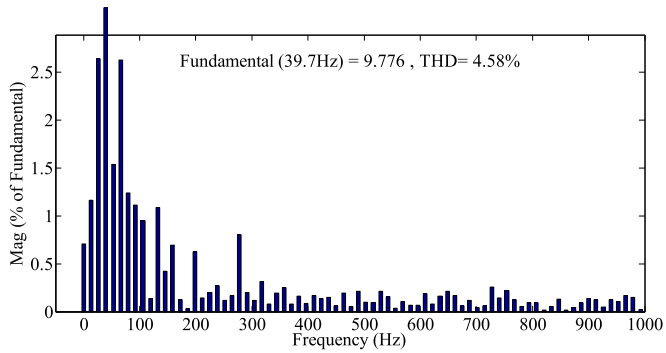

Fig. 27. FFT analysis of the output current of phase A under the improved sampling scheme ($n = 1100$ r/min, $T_e = 9$ N · m).

the speed of 1100 r/min under the load torque of 9 N·m The current waveform is evidently distorted and the motor does not run smoothly with big noise; the corresponding FFT analysis of the current is displayed in Fig. 25, which shows a relatively large THD of 11.51%. On the contrary, the current under the same operation condition turns out to be more sinusoidal and the motor can work well, as shown in Fig. 26, when the improved sampling scheme is used in the control system. Fig. 27 reveals the FFT analysis of the current and the THD is reduced from 11.51% to 4.58%. The results prove that the improved sampling scheme can also make the motor perform well under heavy load.

5) The transient experiments of the new current sampling system are done to verify the performance of the dynamic response. The experiments contain speed transients and load transients. The results are shown in Figs. 28–33. Fig. 28 shows the speed response and the corresponding MI. Fig. 29 shows the load response and the corresponding MI.

In Fig. 28, the speed reference is set to 100 r/min at the beginning of the experiment, 500 r/min at $t = 16$ s, 1300 r/min at $t = 24$ s, 1000 r/min at $t = 59$ s, 500 r/min at $t = 75$ s, and

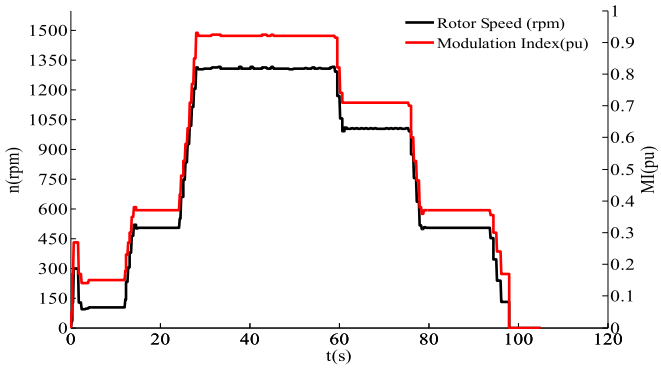

Fig. 28. Speed dynamic experiment under the improved sampling scheme.

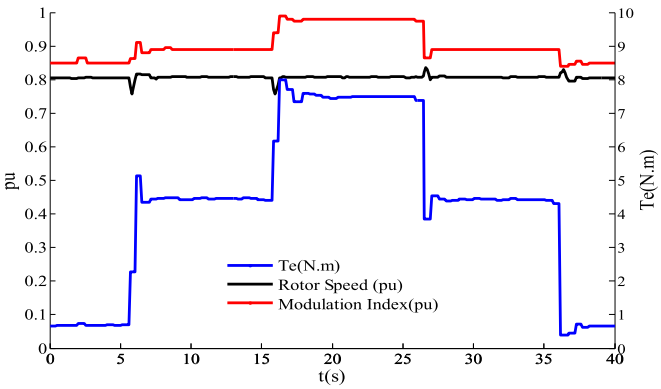

Fig. 29. Torque dynamic experiment under the improved sampling scheme.

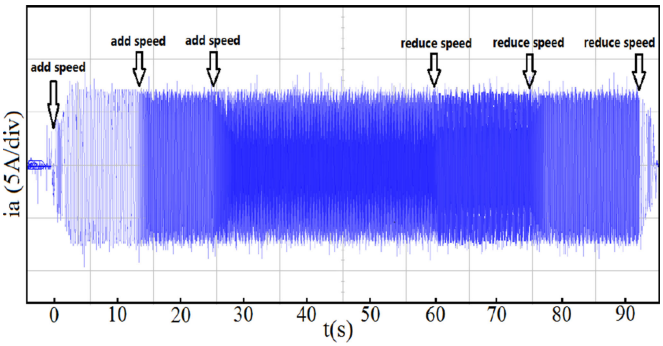

Fig. 30. Corresponding currents of the speed dynamic experiment.

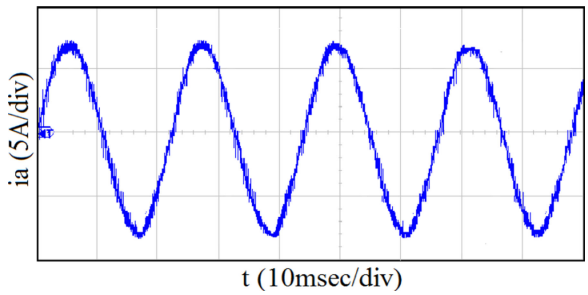

Fig. 31. Zoomed waveform of i_a in the highest MI.

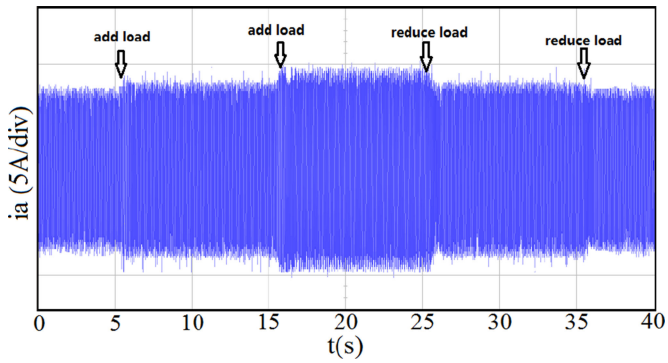

Fig. 32. Corresponding currents of the torque dynamic experiment.

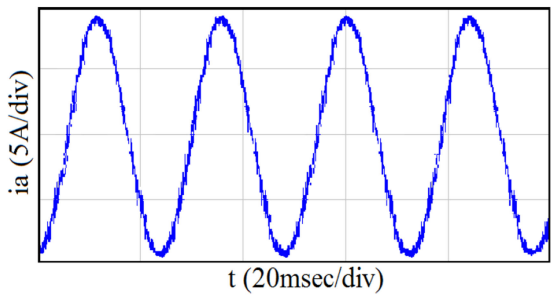

Fig. 33. Zoomed waveform of i_a at the highest MI.

0 r/min at $t = 96$ s. In every stage, the rotor speed can track the reference values very promptly. The current waveform of phase A in the experiment is shown in Fig. 30. Fig. 31 is the zoomed waveform at the highest MI, and there is no distortion of the phase current.

In Fig. 29, for convenience, the speed reference is set to 0.8 pu, which is converted based on 1500 r/min. The initial load torque is 0.7 N·m. At $t = 6$ s, the load is added and the torque rises to 4.5 N·m, and the rotor speed can adjust to the changes and keep the system running at the given value. Next, the load torque is set to 7.6 N·m at $t = 16$ s, 4.5 N·m at $t = 26$ s, and 0.7 N·m at $t = 36$ s. As shown in the figure, the load test includes the increase and the reduction of the load torque. This test shows that the motor works well and the speed keeps stable under various load transients. Because of the limitation of the current protection in the hardware, the maximum MI reaches only 0.98 as the red line shows. From Figs. 32 and 33, the current amplitudes change with the load conditions rapidly and remains sinusoidal under the new sampling method.

VI. Conclusion

This paper proposes an improved three-resistor current sampling scheme based on a predictive current model of the inverter load, in order to overcome the limitation of the traditional method, i.e., reduced MI. When the accurate current sampling becomes impossible at high MIs, the scheme predicts the currents based on the previously obtained values. This approach has been applied to a closed-loop-controlled induction motor

drive and has been tested intensively both in simulation and in experiment. The results show that the scheme can effectively solve the problem and the motor performs well in both steady-state and dynamic conditions when the MI approaches 1 so that the loading capacity of the motor is significantly enhanced. The influence of motor parameters on the improved three-resistor current sampling scheme remains to be further studied in the future.

REFERENCES

[1] M. N. Uddin *et al.*, "Hybrid fuzzy and PID controller based inverter to control speed of AC induction motor," in *Proc. 2015 Int. Conf. Elect. Electron. Eng.*, Rajshahi, 2015, pp. 9–12.

[2] R. A. Kumar and J. L. F. Daya, "A novel indirect field oriented control of induction motor using self-tuning fuzzy PID controller," *Int. J. Syst. Algorithms Appl.*, vol. 3, no. 19, pp. 73–77, Feb. 2013.

[3] R. Ramchand *et al.*, "A current error space vector based hysteresis controller with constant switching frequency and simple online boundary computation for VSI fed IM drive," in *Proc. IECON*, 2010, pp. 729–734.

[4] R. Ramchand *et al.*, "Online computation of hysteresis boundary for constant switching frequency current-error space-vector-based hysteresis controller for VSI-Fed IM drives," *IEEE Trans. Power Electron.*, vol. 27, no. 3, pp. 1521–1529, Mar. 2012.

[5] N. George and S. Gopalakrishna, "An improved anti-differential configuration based hall-effect current sensor," in *Proc. 2016 IEEE Annu. India Conf.*, Bangalore, India, 2016, pp. 1–5.

[6] V. L. Reis *et al.*, "Measuring the excitation current in transformers using hall effect sensors," in *Proc. I2MTC*, 2014, pp. 960–963.

[7] E. M. Esmail, N. I. Elkalashy, T. Kawady, and A. M. I. Taalab, "Experimental implementation of optical current transducers," in *Proc. 2016 18th Int. Middle East Power Syst. Conf.*, Cairo, 2016, pp. 276–281.

[8] S. L. Capecce, C. Cecati, and N. Rotondale, "A sensorless control technique for low cost AC/DC converters," in *Proc. 38th IAS Annu. Meeting Ind. Appl. Conf.*, 2003, vol. 3, pp. 1546–1551.

[9] S. C. Yang, "Saliency-based position estimation of permanent-magnet synchronous machines using square-wave voltage injection with a single current sensor," *IEEE Trans. Ind. Appl.*, vol. 51, no. 2, pp. 1561–1571, Mar.–Apr. 2015.

[10] Y. S. Lai, Y. K. Lin, and C. W. Chen, "New hybrid pulse width modulation technique to reduce current distortion and extend current reconstruction range for a three-phase inverter using only DC-link sensor," *IEEE Trans. Power Electron.*, vol. 28, no. 3, pp. 1331–1337, Mar. 2013.

[11] B. Saritha and P. A. Janakiraman, "Sinusoidal three-phase current reconstruction and control using a DC-link current sensor and a curve-fitting observer," *IEEE Trans. Ind. Electron.*, vol. 54, no. 5, pp. 2657–2664, Oct. 2007.

[12] H. Kim and T. M. Jahns, "Phase current reconstruction for AC motor drives using a DC link single current sensor and measurement voltage vectors," *IEEE Trans. Power Electron.*, vol. 21, no. 5, pp. 1413–1419, Sep. 2006.

[13] H. Lu, X. Cheng, W. Qu, S. Sheng, Y. Li, and Z. Wang, "A three-phase current reconstruction technique using single DC current sensor based on TSPWM," *IEEE Trans. Power Electron.*, vol. 29, no. 3, pp. 1542–1550, Mar. 2014.

[14] Y. Gu, F. Ni, D. Yang, and H. Liu, "Switching-state phase shift method for three-phase-current reconstruction with a single DC-link current sensor," *IEEE Trans. Ind. Electron.*, vol. 58, no. 11, pp. 5186–5194, Nov. 2011.

[15] H. Kim, S. Yi, N. Kim, and R. D. Lorenz, "Using low resolution position sensors in bumpless position/speed estimation methods for low cost PMSM drives," in *Proc. 40th IAS Annu. Meeting*, 2005, vol. 4, pp. 2518–2525.

[16] S. Chi *et al.*, "A current reconstruction scheme for low-cost PMSM drives using shunt resistors," in *Proc. APEC*, 2007, pp. 1701–1706.

[17] S. N. Misti *et al.*, "A new trimming approach for shunt resistors used in metering applications," in *Proc. 2014 2nd Int. Conf. Electron. Design*, Penang, 2014, pp. 94–99.

[18] G. Q. Yu, Y. Zhang, and Y. w. Li, "Research of DSP-based SVPWM vector control system of asynchronous motor," in *Proc. 2012 Int. Conf. ICCSEE*, Hangzhou, China, 2012, pp. 151–155.

[19] R. J. Lee, P. Pillay, and R. G Harley, "D,Q reference frames for the simulation of induction motor," *Electr. Power Syst. Res.*, vol. 8, no. 1, pp. 15–26, 1984.

[20] M. Datta, M. A. Rafiq, and B. C. Ghosh, "Genetic algorithm based fast speed response induction motor drive without speed encoder," in *Proc. 2007 Int. Conf. Power Eng., Energy Elect. Drives*, Setubal, Portugal, 2007, pp. 146–151.

Ziyi Li received the B.Sc. degree in electrical engineering from the South China University of Technology, Guangzhou, China, in 2014, and the M.Sc. degree, majored in the power electronics, electric machines, and drives, from Shanghai Jiao Tong University (SJTU), Shanghai, China, in 2017.

Since graduation from SJTU, he has been with Huawei Technologies Co., Ltd., Shanghai, China, as an R&D Engineer. His current research interest is photovoltaic inverters.

Qiang Gao received the B.Sc. and M.Sc. degrees in electrical engineering from Shanghai Jiao Tong University (SJTU), Shanghai, China, and the Ph.D. degree from the University of Nottingham (UoN), Nottingham, U.K.

After receiving the M.Sc degree, from 2001 to 2003, he was an R&D Engineer with the Delta Power Electronics Centre, Delta Electronics, Shanghai. From 2006 to 2009, he was with the Department of Electrical and Electronic Engineering, UoN, working as a Research Fellow on PMSM's sensorless control using matrix converter. In October 2009, he joined the Wind Power Research Centre and the Department of Electrical Engineering, SJTU, and was appointed as an Associate Professor. His current research interests include electric machines and drives, power converters, and wind power generation.